Materials Science and Engineering B 303 (2024) 117296

Contents lists available at ScienceDirect

Materials Science & Engineering B

journal homepage: www.elsevier.com/locate/mseb

# Improving the performance of $Cu_2ZnSn(S,Se)_4$ thin film solar cells by SCAPS simulation

Yaowei Wei [a,*], Zhao Ma [a], Xiaoyang Zhao [a,b], Jianghao Yin [a], Yingying Wu [a], Leng Zhang [c,*], Ming Zhao [d,*]

[a] State Center for International Cooperation on Designer Low-Carbon & Environmental Materials (CDLCEM), School of Materials Science and Engineering, Zhengzhou University, Zhengzhou 450001, China
[b] Engineering Research Center for Semiconductor Integrated Technology, Institute of Semiconductors, Chinese Academy of Sciences, Beijing 100083, China
[c] School of Electronics and Information Engineering, Jinling Institute of Technology, Nanjing 211169, China
[d] Key Lab for Advanced Materials Processing Technology of Ministry of Education, School of Materials Science and Engineering, Tsinghua University, Beijing 100084, China

ARTICLE INFO

*Keywords:*
CZTSSe solar cell
SCAPS-1D
Se/(S+Se) ratio
Absorber thickness
Series resistance
Shunt resistance

ABSTRACT

The effect of Se/(S + Se) ratio, absorber thickness, series and shunt resistance on $Cu_2ZnSn(S,Se)_4$ (CZTSSe) solar cells were studied by one-dimensional solar cell capacitance simulator (SCAPS-1D). The efficiency exhibited an initial increase followed by a subsequent decrease as Se/(S + Se) ratio increased, achieving peak efficiency of 17.38 % at Se/(S + Se) ratio of 0.2. As absorber thickness increased from 0.5 to 1.5 μm, both the short circuit current and efficiency exhibited continuous improvement, which was attributed to the enhanced absorption and utilization of sunlight. However, when the thickness of absorber exceeded 1.5 μm, the transport of carriers across the absorber was difficult due to the excessive thickness, and the efficiency was almost not improved. The optimal device possessed efficiency of 17.91 %. Series resistance exerted a more substantial influence on efficiency than shunt resistance. To achieve high-efficiency CZTSSe devices, series resistance should be controlled below 2 $\Omega\cdot cm^2$, and shunt resistance should be controlled above 600 $\Omega\cdot cm^2$.

## 1. Introduction

Solar cells can convert solar energy into electricity through the photovoltaic effect of pn junction [1–3]. Thin film solar cells have a high optical absorption coefficient, requiring only a few micrometers of thickness for adequate light absorption [4–6]. The small thickness makes it easy to bend, enabling the production of flexible solar cells for curved surfaces in vehicles and flexible surfaces in wearable devices. They can also be used to fabricate ultrathin and semitransparent solar cells by reducing the thickness of absorber, with promising applications in building integrated photovoltaics (BIPV) [7,8].

The mixed chalcogenide $Cu_2ZnSn(S,Se)_4$ (CZTSSe), composed of earth-rich, low-cost, and eco-friendly elements [9,10], demonstrates impressive photovoltaic performance and stands out as a promising absorber material for third-generation kesterite-based thin film solar cells [11]. CZTSSe has two structures Kesterite and Stannite [12]. Due to the low energy and relative stability of the Kesterite phase, CZTSSe mostly exists in the form of the kesterite phase [13]. CZTSSe exhibits a direct bandgap semiconductor with adjustable band gaps ($E_g$) ranging from 1.0 to 1.5 eV [14,15] and a notably high optical absorption coefficient exceeding $10^4$ $cm^{-1}$ [16,17]. CZTSSe solar cells are thin film solar cells derived from $Cu(In,Ga)Se_2$ (CIGS) solar cells, and the theoretical power conversion efficiency (PCE) of CZTSSe solar cells is 33.7 % according to Shockley-Queisser theoretical calculations [18,19]. In recent years, extensive research efforts have been dedicated to improving the efficiency of CZTSSe solar cells. Remarkable achievements have been attained in the efficiency of CZTSSe solar cells, but the highest recorded PCE for CZTSSe solar cells has only reached 13.8 % [20], which is considerably lower than the theoretical conversion efficiency.

The physical properties of CZTSSe absorber are markedly influenced by its composition. One of the key factors is the Se and S content within the absorber, which determines the elemental stoichiometry of CZTSSe. Changes in chemical composition can lead to significant alterations in the physical properties of band gaps and optical absorption coefficients, both of which play pivotal roles in the performance of solar cells. The band gaps for CZTSe and CZTS are 1.0 eV and 1.5 eV, respectively.

* Corresponding authors.
*E-mail addresses:* ywwei@zzu.edu.cn (Y. Wei), zhangleng2018@jit.edn.cn (L. Zhang), zhaoming2013@mail.tsinghua.edu.cn (M. Zhao).

https://doi.org/10.1016/j.mseb.2024.117296
Received 23 December 2023; Received in revised form 11 February 2024; Accepted 28 February 2024
Available online 11 March 2024

Therefore, the band gaps and optical absorption coefficients of CZTSSe are intricately determined by the composition and can be adjusted by varying the Se/(S + Se) ratio [21,22]. Additionally, CZTSSe absorbers possess high optical absorption coefficients, allowing them to capture a substantial portion of sunlight even with minimal thickness. However, when the absorber is excessively thin, it results in inadequate light absorption. Conversely, an overly thick absorber raises material preparation costs. Furthermore, the increased demand for carrier transport with excessive absorber thickness contributes to heightened carrier recombination [23,24]. Therefore, establishing the optimal thickness for the absorber is crucial to seek a balance between manufacturing costs and the conversion efficiency of CZTSSe solar cells. In solar cells, series and shunt resistances are important factors affecting the device performance. Series resistance is closely associated with non-ideal contacts between individual layers and the inherent resistance of each material [25,26]. Shunt resistance is typically influenced by non-ideal pn junction or impurities near the junction, resulting in unexpected shunting current within the pn junction [27]. Therefore, it is necessary to find the appropriate range of series resistance and shunt resistance to obtain high-efficiency solar cells.

In this study, the potential efficiencies of CZTSSe solar cells were examined using the one-dimensional solar cell capacitance simulator (SCAPS-1D). Initially, a model of a CZTSSe solar cell was established with a structure comprising Mo/p-CZTSSe/n-CdS/i-ZnO/ZnO:Al. The accuracy of the model underwent validation through a comparative analysis of its performance against actual cells. Subsequently, the effects of absorber Se/(S + Se) ratio, absorber thickness, series resistance, and shunt resistance on solar cell performance were studied. This study provides substantial theoretical insights for the production of high-efficiency CZTSSe solar cells.

## 2. Parameters and methodology

SCAPS-1D is a one-dimensional solar cell capacitance simulation program devised by the University of Gent, Belgium, which was initially developed to study the structure of $CuInSe_2$ and CdTe cells [28]. SCAPS-1D can be used to establish solar cell models, which can shorten the research period and reduce research costs. Recently, SCAPS-1D has been applied to simulate various solar cells [29,30]. SCAPS-1D can build a more realistic solar cell model by considering the effects of defect types, internal cell recombination mechanisms, resistance, and other factors. Therefore, the cell model obtained through SCAPS-1D simulation closely approximates actual cell performance. It is a convenient and efficient research method that provides theoretical guidance for experiments. The working principle of SCAPS-1D involves solving the Poisson Eq. (1), the electron continuity Eq. (2), and the hole continuity Eq. (3) based on material parameters [31,32].

$$\frac{\partial^2 \Psi}{\partial x} + \frac{q}{\varepsilon}\left[p(x) - n(x) + N_D^+ - N_A^- + \rho(n,p)\right] = 0 \quad (1)$$

$$\frac{1}{q}\frac{dJ_n}{dx} = -G_{op}(x) + R(x) \quad (2)$$

$$\frac{1}{q}\frac{dJ_p}{dx} = G_{op}(x) - R(x) \quad (3)$$

where $\Psi$ is the $x$-dependent electrostatic potential function, $q$, $\varepsilon$, $\rho$ are the electron charge, the permittivity and the defect charge density, respectively, $n$ and $p$ are the electron and hole concentrations, $N_D^+$ and $N_A^-$ are the densities of the ionized donors and acceptors, $J_n$ and $J_p$ are the electron and hole current densities, $G_{op}$ is the carrier generation rate under illumination, and $R$ is the rate of direct and indirect recombination.

CZTSSe solar cells were modeled utilizing SCAPS-1D based on actual cells with structure of Mo/p-CZTSSe/n-CdS/i-ZnO/ZnO:Al, as shown in Fig. 1**(a)**. The Mo layer is the back electrode layer, CZTSSe is a p-type light absorption layer, CdS is an n-type buffer layer, i-ZnO is the intrinsic layer and ZnO:Al is the window layer. The material parameters of each layer of solar cells set in SCAPS-1D were derived from the literature [33–37], as shown in Table 1. The illumination used is the standard AM 1.5 G spectrum, and the light intensity was set to 1000 W/m$^2$ [38], as shown in Fig. 1**(b)**. The electron and hole capture cross-sections were both set to $1 \times 10^{15}$ cm$^2$, and the interface defects were not considered temporarily [39]. The work function of the back contact Mo was set as 5

**Table 1**
Material parameters of CZTSSe solar cell.

| Device parameters | CZTSSe | CdS | i-ZnO | ZnO:Al |
|---|---|---|---|---|
| Thickness (nm) | 1000 | 50 | 50 | 300 |
| $E_g$ (eV) | 1.09 | 2.4 | 3.3 | 3.3 |
| $\chi$ (eV) | 4.18 | 4.2 | 4.4 | 4.4 |
| $\varepsilon$ | 13.6 | 10 | 9 | 9 |
| $N_c$ (cm$^{-3}$) | $2.2 \times 10^{18}$ | $2.2 \times 10^{18}$ | $2.2 \times 10^{18}$ | $2.2 \times 10^{18}$ |
| $N_v$ (cm$^{-3}$) | $1.8 \times 10^{19}$ | $1.8 \times 10^{19}$ | $1.8 \times 10^{19}$ | $1.8 \times 10^{19}$ |
| $\mu_n$ (cm$^2$/Vs) | 100 | 100 | 100 | 100 |
| $\mu_p$ (cm$^2$/Vs) | 25 | 25 | 25 | 25 |
| $\nu_{t-h}$ (cm/s) | $1.0 \times 10^7$ | $1.0 \times 10^7$ | $1.0 \times 10^7$ | $1.0 \times 10^7$ |
| $\nu_{t-e}$ (cm/s) | $1.0 \times 10^7$ | $1.0 \times 10^7$ | $1.0 \times 10^7$ | $1.0 \times 10^7$ |
| $N_A$ (cm$^{-3}$) | $1.0 \times 10^{17}$ | – | $1.0 \times 10^{19}$ | – |
| $N_D$ (cm$^{-3}$) | – | $1.0 \times 10^{18}$ | $1.0 \times 10^{19}$ | $1.0 \times 10^{20}$ |
| Defect concentration (cm$^{-3}$) | $1.0 \times 10^{17}$ | $1.0 \times 10^{17}$ | $1.0 \times 10^{17}$ | $1.0 \times 10^{17}$ |

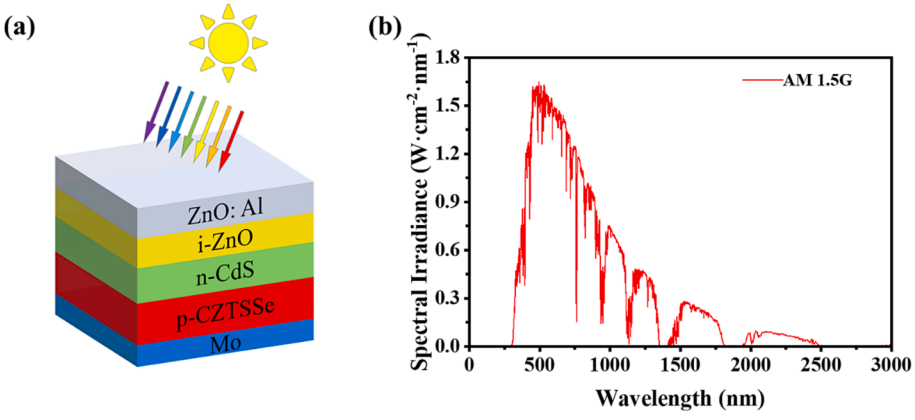


**Fig. 1.** (a) Structure of CZTSSe solar cell, and (b) radiation intensity of AM 1.5 G spectrum in SCAPS-1D.

eV [40], and the environmental temperature was set to 300 K.

After establishing the solar cell model, the accuracy of the model was initially verified by comparing its performance with that of the actual device. Subsequently, the Se/(S + Se) ratios for the absorbers were sequentially set to 0.0, 0.2, 0.4, 0.6, 0.8 and 1.0, respectively. The associated band gaps and optical absorption coefficients of absorbers were obtained, and the current–voltage (*J-V*) curves, efficiencies, external quantum efficiency (EQE) curves, and integrated currents of devices with varying components were studied. Then the obtained optimal Se/(S + Se) ratio was applied, and the absorber thicknesses were varied at 0.5, 1.0, 1.5, 2.0, 2.5, and 3.0 μm, respectively. The correlation between device performance and absorber thickness was investigated to achieve a balance between enhanced light absorption and minimized carrier recombination with increasing absorber thickness. Finally, the optimized Se/(S + Se) ratio and absorber thickness were utilized, and the effects of series resistance and shunt resistance on device performance were explored through the equivalent circuit model of solar cells.

## 3. Results and discussion

### 3.1. Assessing the feasibility of SCAPS-1D simulation

Material parameters for each layer of solar cell were defined based on Table 1. Following the establishment of the CZTSSe device model, it is essential to validate the accuracy before proceeding with additional experiments. A performance comparison between the CZTSSe device model developed in this study and the actual device reported in the literature [41] was carried out. The *J-V* curves and comprehensive performance parameters are presented in Table 2. The simulated *J-V* curve closely mirrors the experimental *J-V* curve in trend. The open-circuit voltage ($V_{oc}$), short circuit current ($J_{sc}$), fill factor (FF), and PCE also exhibit close approximation. The CZTSSe device model simulated using SCAPS-1D is accurate and operationally feasible, providing a dependable guide for experimental endeavors.

### 3.2. Effect of selenium content of CZTSSe absorber on cell performance

Fig. 2 illustrates the influence of selenium content on band gap and optical absorption coefficient. Fig. 2**(a)** displays the band gaps of absorbers with varying selenium contents. The conventional preparation method for a CZTSSe absorber involves initially preparing a CZTS precursor film and subsequent selenization annealing treatment. During this process, some sulfur (S) in CZTS is substituted with homologous selenium (Se), and the selenium content is expressed as the Se/(S + Se) ratio. CZTSe is formed when Se completely replaces S. The band gaps of CZTS and CZTSe are 1.5 eV and 1.0 eV, respectively. Variations in the Se/(S + Se) ratio lead to the band gap of CZTSSe ranging between 1.0 and 1.5 eV. The band gap of CZTSSe with different selenium content can be determined using the Vegard's Law [42,43]:

$$E_g(x) = (1-x)E_g(\mathrm{CZTS}) + xE_g(\mathrm{CZTSe}) - bx(1-x) \quad (4)$$

where $x$ is the Se/(S + Se) ratio, and b is the bending factor utilized to characterize the degree of nonlinearity, with a value of approximately 0.08 eV [44]. The Se/(S + Se) ratios $x$ are set at 0.0, 0.2, 0.4, 0.6, 0.8, and 1.0, respectively. The obtained band gaps are 1.5, 1.39, 1.28, 1.18, 1.09, and 1.0 eV, respectively. Given the small value of the bending coefficient, the variation in the band gap of the absorber is approximately linear. As the selenium content increases, the band gap of CZTSSe gradually converges towards that of CZTSe, rendering it more effective in absorbing sunlight in the long-wavelength range.

**Table 2**
Performance of solar cells in actual experiments and simulation.

| Cell | $V_{oc}$ (V) | $J_{sc}$ (mA/cm$^2$) | FF (%) | PCE (%) |
|---|---|---|---|---|
| CZTSSe (Literature) [41] | 0.521 | 34.98 | 67.2 | 12.3 |
| CZTSSe (Simulation) | 0.560 | 36.18 | 62.8 | 12.6 |

Fig. 2**(b)** illustrates the absorption coefficients of CZTSSe with varying selenium contents. Assuming that CZTSSe absorber possesses uniform composition distribution, the optical absorption coefficient of CZTSSe with different selenium contents can be calculated using Eq. (5) [45]:

$$log\alpha(\lambda) = (1-x)log\alpha_{CZTS}(\lambda) + xlog\alpha_{CZTSe}(\lambda) \quad (5)$$

where $\alpha(\lambda)$ is the optical absorption coefficient of CZTSSe. The absorption coefficient exhibits a gradual increase with the rise in selenium content, particularly in the visible light range of 400–700 nm. As the band gap of the absorber decreases, the absorption coefficient increases, thereby facilitating sunlight absorption and enhancing photo-generated current within a specific range.

Fig. 3 shows the impact of selenium content on the performance of CZTSSe cells. Fig. 3**(a)** presents the *J-V* curves of CZTSSe cells with varying Se/(S + Se) ratios, and the specific parameters of the solar cells are detailed in Table 3. The $J_{sc}$ increases from 28.78 mA/cm$^2$ to 40.00 mA/cm$^2$ with the rise in the Se/(S + Se) ratio, indicating a proportional relationship with selenium content. Conversely, the $V_{oc}$ decreases from 0.97 V to 0.48 V, demonstrating an inverse relationship with selenium content. A CZTSe cell exhibits high $J_{sc}$, whereas a CZTS cell demonstrates high $V_{oc}$. The FF reflects the fullness of the *J-V* curve. As the Se/(S + Se) ratio increases from 0.0 to 1.0, the FF of CZTSSe cells initially rises from 60.86 % to 68.09 % and subsequently decreases to 59.40 %. When the Se/(S + Se) ratio increases at low value, the positive effect of the increase of open circuit voltage on FF at the beginning is greater than the negative effect of the decrease of short circuit current. However, when the selenium to sulfur ratio increases further, the decrease of short circuit current has a greater negative effect on FF than the positive effect of the increase of open circuit voltage. Moreover, the recombination rate of carriers also increases, which causes a further decline in FF. Through the adjustment of Se/(S + Se) ratios, CZTSSe cells can attain relatively high $V_{oc}$, $J_{sc}$, and FF, thereby significantly enhancing device efficiency. Fig. 3**(b)** depicts the efficiencies of CZTSSe solar cells with varying Se/(S + Se) ratios. As the selenium content increases, the cell efficiency initially rises from 17.01 % to 17.38 % and subsequently decreases to 11.43 %. The champion device with $V_{oc}$ of 0.85 V, $J_{sc}$ of 30.10 mA/cm$^2$, FF of 68.09 %, and efficiency of 17.38 % is achieved when Se/(S + Se) ratio is 0.2.

Fig. 4**(a)** illustrates EQE curves of CZTSSe solar cells with different Se/(S + Se) ratios. The EQE curve illustrates the spectral responses of solar cells to different wavelengths of light. The area beneath the EQE curve is proportional to solar spectral absorption and therefore proportional to the output current. The CZTSSe device with a Se/(S + Se) ratio of 0.0 exhibits the lowest EQE. With the increase of selenium content, the EQE for medium and long wave gradually increases, leading to enhanced absorption of sunlight in these ranges by the absorber. The CZTSSe device with a Se/(S + Se) ratio of 1.0 exhibits a high EQE curve, reflecting heightened spectral responses from visible to near-infrared regions. As depicted in Fig. 4**(b)**, the $J_{sc}$ obtained by integrating EQE from Fig. 4**(a)** aligns with the measured device performance.

Fig. 5 displays the energy level diagrams of reference and optimal CZTSSe solar cells. The consistency of band gap energy is crucial in determining the performance of heterojunctions. In Fig. 5**(a)**, the Se/(S + Se) ratio of the reference CZTSSe absorber is 0.8, and the band gap is 1.09 eV. The Se/(S + Se) ratio of the optimal absorber is 0.2, and the band gap is 1.39 eV, which is closer to that of the CdS buffer. The valence band offset between the absorber and buffer for the reference sample is 1.3 eV, which is reduced to 1.1 eV for the optimal sample. The decrease of valence band offset is beneficial to the transport of photo-generated holes and leads to the decrease of the electric field strength of the semiconductor, thus reducing the recombination probability between the photo-generated holes and the electrons, and the holes are easier to

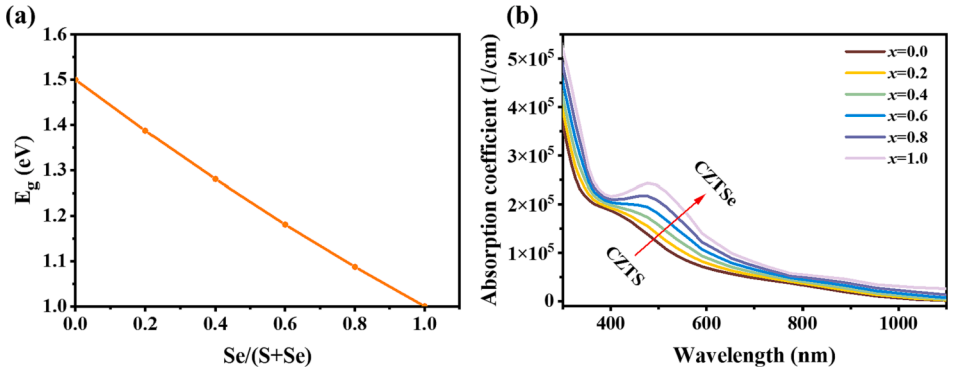


**Fig. 2.** (a) Band gap and (b) optical absorption coefficients of absorbers with different Se/(S + Se) ratio.

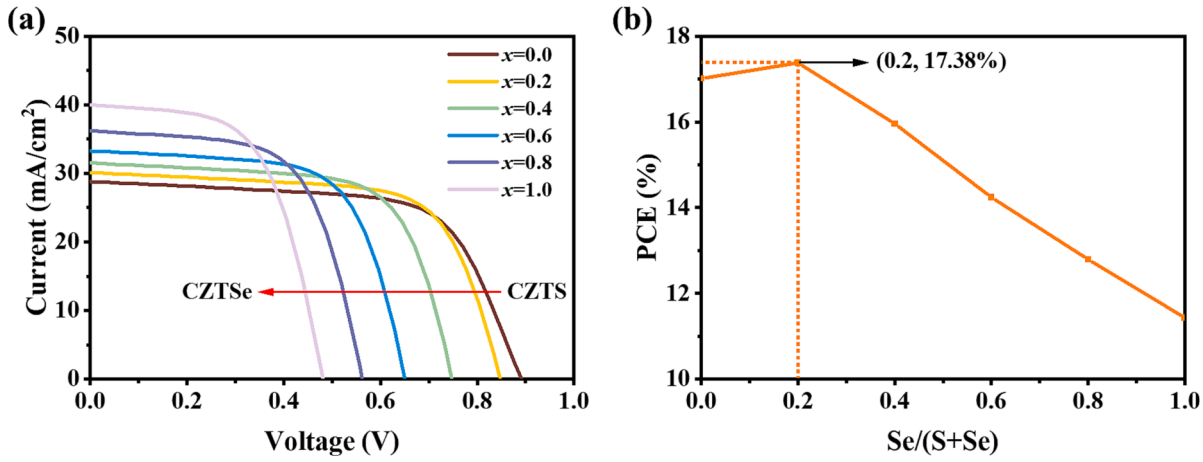


**Fig. 3.** (a) *J-V* curves, and (b) PCE of CZTSSe solar cells with different Se/(S + Se) ratios.

**Table 3**
Performance parameters of CZTSSe cells with different Se/(S + Se).

| Se/(S + Se) | $V_{oc}$ (V) | $J_{sc}$ (mA/cm$^2$) | FF (%) | PCE (%) |
|---|---|---|---|---|
| 0.0 | 0.97 | 28.78 | 60.86 | 17.01 |
| 0.2 | 0.85 | 30.10 | 68.09 | 17.38 |
| 0.4 | 0.74 | 31.50 | 67.62 | 15.86 |
| 0.6 | 0.64 | 33.28 | 65.58 | 14.13 |
| 0.8 | 0.56 | 36.18 | 62.78 | 12.60 |
| 1.0 | 0.48 | 40.00 | 59.40 | 11.43 |

migrate to the semiconductor surface [46,47]. Although the increase of conduction band offset will make the transport capacity of photo-generated electrons worse, the increase of conduction band offset can increase the intensity of the built-in electric field, inhibit the generation of reverse dark current, and increase the open circuit voltage and fill factor of the solar cell. In Fig. 5**(b)**, "spikes" and "notches" are observed between the buffer and intrinsic ZnO layer. The "spike" is a potential barrier for electrons, resulting in a decrease in potential and increases electron potential energy. The "notch" is a trap for electrons, which has low potential energy. The "spike" has the role of driving out electrons, while the "notch" has the role of driving out holes and accumulating electrons. These two actions cause electrons to gather in the "notch". There is no obvious "spike" and "notch" in the reference sample, because the band structure has not reached the best matching degree, and the energy difference between the bottom of the conduction band and the top of the valence band is still large, resulting in the degree of band bending is not obvious. Such band structure results in low carrier transport efficiency and high carrier recombination rate. Due to the scattering effect of ionized impurities, charge carriers are subjected to Coulomb forces when passing near the impurity ions, leading to alterations in motion state and reduced mobility, which is not conducive to the transport of carriers. Electrons accumulate at the intrinsic ZnO, which does not contain ionized impurities, thereby enhancing electron mobility and facilitating carrier transport.

### 3.3. Impact of absorber thickness on performance of CZTSSe cells

The absorption rate of sunlight by the absorber is primarily dependent on the band gap and the thickness of absorber. The Se/(S + Se) ratio that affects the band gap is fixed at the optimal value of 0.2 based on the peak efficiency device. To explore the effects of absorber thicknesses on CZTSSe device performance, the absorber thicknesses are set to 0.5, 1.0, 1.5, 2.0, 2.5, and 3.0 μm, respectively. The other parameters of the CZTSSe cell are still set according to Table 1.

Fig. 6 shows the performance of CZTSSe cells with different absorber thicknesses. In Fig. 6**(a)**, the influence of absorber thickness on $V_{oc}$ is not significant, especially when $V_{oc}$ remains essentially unchanged when the thickness exceeds 1.5 μm. In Fig. 6**(b)**, the $J_{sc}$ increases from 26.61 mA/cm$^2$ to 30.91 mA/cm$^2$ as the absorber thickness increases from 0.5 μm to 1.5 μm. However, the $J_{sc}$ only increases to 31.18 mA/cm$^2$ when the thickness reaches 3.0 μm. When the thickness is greater than 1.5 μm, the increase in $J_{sc}$ is slight, as the absorption of light reaches saturation with adequate absorber thickness. In Fig. 6**(c)**, the FF increases from 67.51 % to 68.05 % and then decreases slightly to 67.97 % with the increase of absorber thickness. When the CZTSSe thickness is small, the light absorption is insufficient and the short circuit current is small, resulting in a low FF. As the CZTSSe thickness increases, the light absorption enhances and the short circuit current increases, resulting in the increase of FF. However, When the thickness of CZTSSe further increases to more

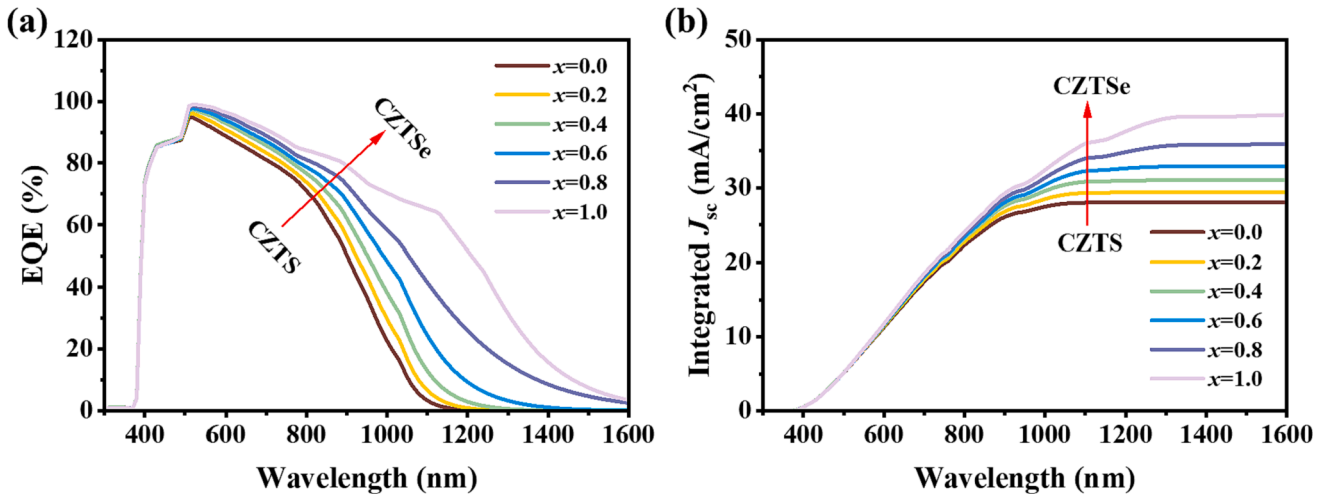


**Fig. 4.** (a) EQE curves, and (b) integrated $J_{sc}$ of CZTSSe solar cells with different Se/(S + Se) ratios.

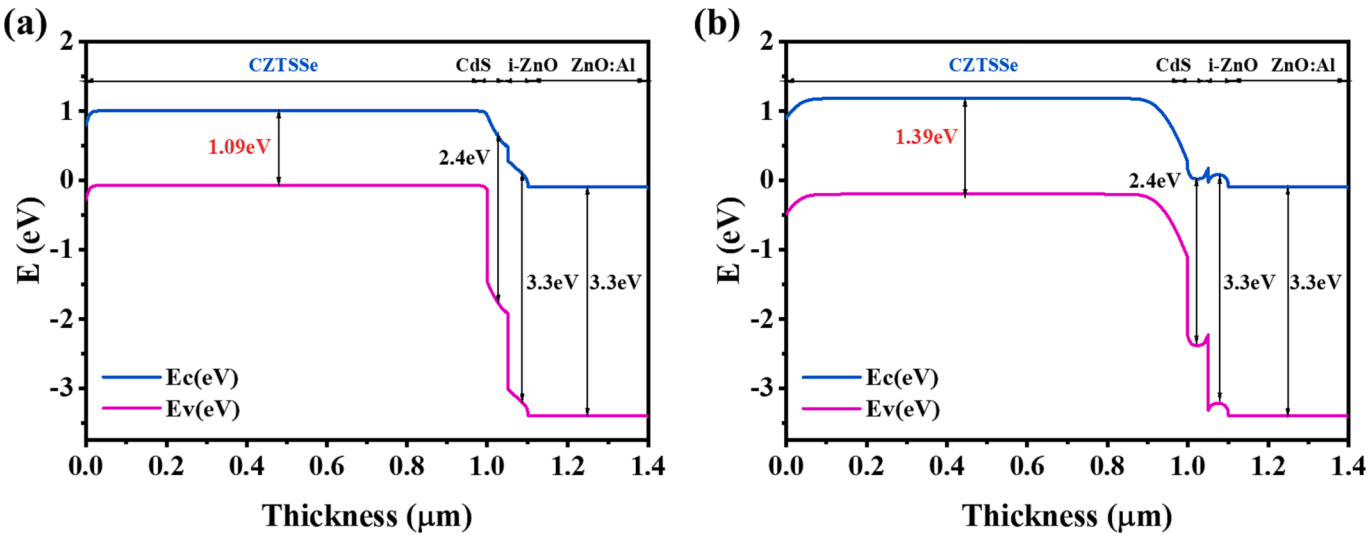


**Fig. 5.** Energy level diagrams of (a) reference and (b) optimal CZTSSe solar cells.

than 1.5 μm, the light absorption is saturated but the transport distance required for the photo-generated carriers increases, resulting in the decrease of FF. In Fig. 6**(d)**, PCE increases gradually from 15.03 % to 17.91 % with the increase of thickness from 0.5 μm to 1.5 μm, which is mainly due to the increase in $J_{sc}$ caused by light absorption. When the thickness exceeds 1.5 μm, the increase in PCE is insignificant with relatively adequate light absorption. PCE only increases to 18.09 % when the thickness increases to 3.0 μm.

Fig. 7 shows the effects of absorber thickness on *J-V* and EQE curves. In Fig. 7**(a)**, with the increase of absorber thickness, $J_{sc}$ increases significantly and $V_{oc}$ increases slowly. When the thickness exceeds than 1.5 μm, the *J-V* curves of different devices are very close, indicating that the performance improvement is insignificant. The enhancement of sunlight utilization by increasing the thickness of the absorber beyond 1.5 μm is basically counteracted by the increase in carrier recombination. The device with $V_{oc}$ of 0.85 V, $J_{sc}$ of 30.91 mA/cm$^2$, FF of 68.05 %, and PCE of 17.91 % is obtained when the thickness is 1.5 μm. In Fig. 7 **(b)**, the $J_{sc}$ obtained by integrating from EQE is well matched with the measured device performance. With the increase of CZTSSe absorber thickness, the EQE increases, indicating an improvement in the absorption of photons above 500 nm. When the absorber is too thin, increasing the thickness will cause multiple reflections and scattering of photons in the absorber, thereby increasing the effective interaction time and path of photons with the absorber, improving the light absorption rate and the generation rate of photogenerated carriers. It will also enhance the built-in electric field in the absorber, thereby increasing the drift velocity and directionality of carriers in the absorber, reducing the diffusion length and time of carriers in the absorber, lowering the collision probability of carriers with defects or impurities at the interface, and reducing the defect recombination at the interface. When the absorber is too thick, the transport distance required for the photo-generated carriers increases. Once the absorber thickness exceeds the transport distance of carriers, the transport of carriers across the absorber becomes difficult. Moreover, the excessive thickness of the absorber will increase the concentration gradient of carriers and the recombination of carriers greatly increases, which will worsen the cell performance. After the absorber thickness exceeds 1.5 μm, the improvement of EQE is not significant, because the absorption of light by the absorber increases very little, but the recombination of carrier increases. Moreover, the material cost rises with the increase of thickness. Therefore, it is necessary to consider the contradiction between cell performance and material cost. The optimal thickness of the absorber should be 1.5 μm, which is basically consistent with the actual thickness of the CZTSSe absorber [48–50].

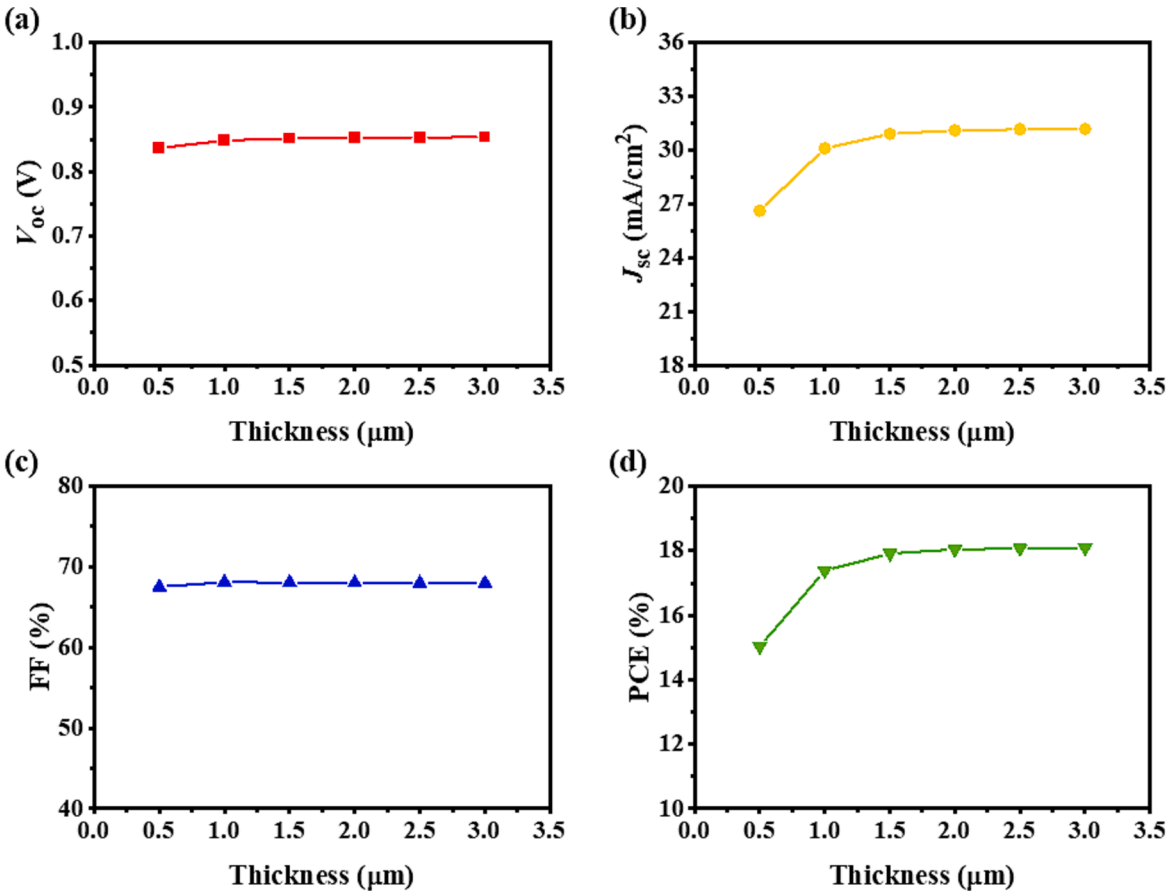


**Fig. 6.** Performance parameters of CZTSSe cells with different absorber thicknesses: (a) $V_{oc}$, (b) $J_{sc}$, (c) FF, and (d) PCE.

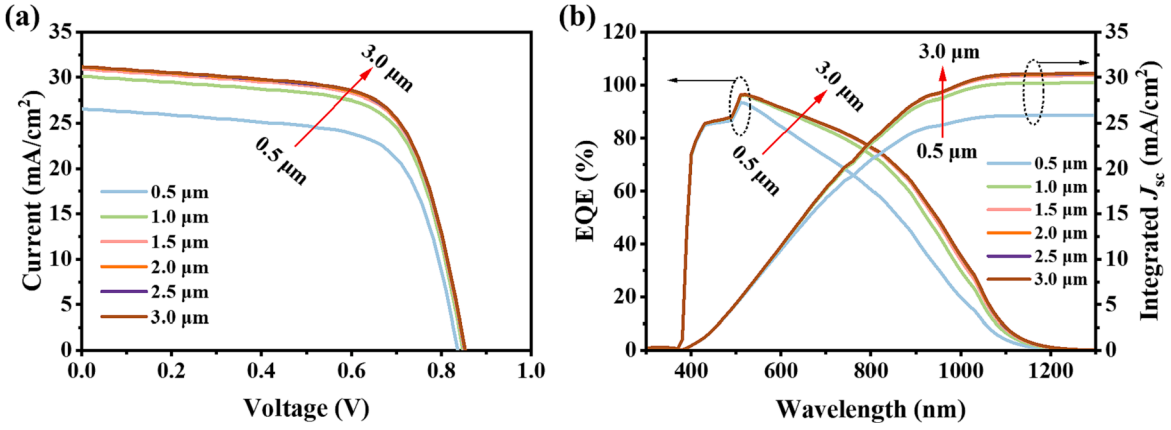


**Fig. 7.** (a) *J-V* and (b) EQE curves of CZTSSe cells with different absorber thicknesses.

### 3.4. Impact of series and shunt resistance on cell performance

The solar cell under illumination conditions can be considered as a constant current source in parallel to an ideal diode, and its equivalent circuit representation is illustrated in Fig. 8 [51]. $I_{ph}$ is photo-generated current, $R_s$ is series resistance, $R_{sh}$ is shunt resistance, and $R$ is external load. In solar cells, series and shunt resistance are important factors affecting device performance. Series resistance is related to the non-ideal contact of metal–semiconductor and the resistance of each material. Shunt resistance is usually affected by non-ideal pn junction or impurities near the junction, which results in shunting current in the pn junction.

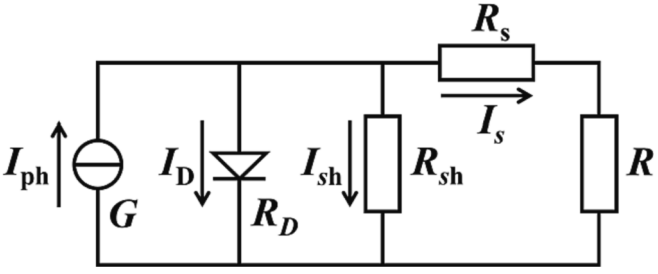


**Fig. 8.** Equivalent circuit diagram of CZTSSe solar cell.

To investigate the effects of $R_s$ and $R_{sh}$ on device performance, the Se/(S + Se) ratio and absorber thickness were fixed at the optimal values of 0.2 and 1.5 μm, respectively. The values of $R_s$ and $R_{sh}$ were changed from 0 to 20 Ω·cm$^2$ and from 300 to 1500 Ω·cm$^2$, respectively. Fig. 9 illustrates the effects of $R_s$ and $R_{sh}$ on the performance of solar cells. Fig. 9**(a)** shows that $V_{oc}$ is nearly unaffected by $R_s$, but positively correlated with $R_{sh}$. In Fig. 9**(b)**, when $R_{sh}$ is small, $J_{sc}$ is significantly influenced by $R_s$ and is inversely proportional to $R_s$. When $R_{sh}$ is large, $J_{sc}$ is less affected by $R_s$. Only when $R_s$ is large, $J_{sc}$ is significantly affected by $R_{sh}$. In Fig. 9**(c)**, FF is insensitive to $R_{sh}$ but inversely proportional to $R_s$. Fig. 9**(d)** shows the effects of $R_s$ and $R_{sh}$ on the PCE of solar cells. $R_s$ has a greater impact on PCE than $R_{sh}$, and PCE is negatively correlated with $R_s$. To realize CZTSSe solar cells with high efficiency, the series resistance should be controlled below 2 Ω·cm$^2$, and shunt resistance should be controlled above 600 Ω·cm$^2$. Fig. 10, illustrates the EQE curve and integrated $J_{sc}$ of CZTSSe cells with series resistance of 2 Ω·cm$^2$ and shunt resistance of 600 Ω·cm$^2$. The EQE data reflects the high spectral responses from visible to near-infrared regions.

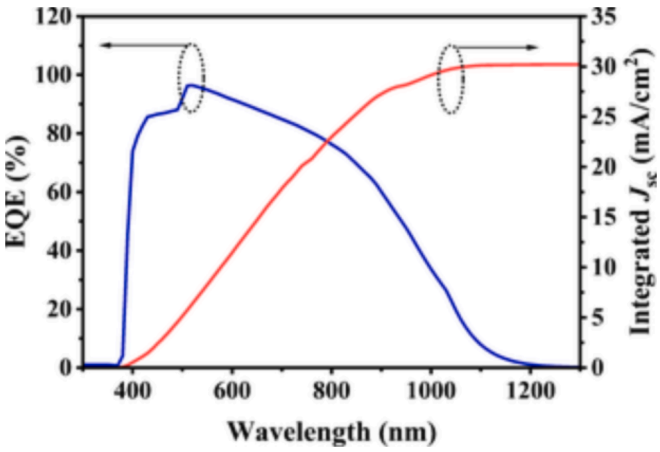


**Fig. 10.** EQE curve and integrated $J_{sc}$ of CZTSSe cells with series resistance of 2 Ω·cm$^2$ and shunt resistance of 600 Ω·cm$^2$.

## 4. Conclusion

In this work, a CZTSSe solar cell model with the structure of Mo/p-CZTSSe/n-CdS/i-ZnO/ZnO:Al was established utilizing SCAPS-1D, and the accuracy of the model was validated by comparing the cell model with previous actual experimental cells. The effects of absorber Se/(S + Se) ratio, absorber thickness, series resistance, and shunt resistance on photovoltaic performance were studied. When the Se/(S + Se) ratio is 0.2, the band gap of the CZTSSe absorber is 1.39 eV, achieving a solar cell with an efficiency of 17.38 %. Increasing the thickness of the CZTSSe absorber can improve the absorption of sunlight, thereby improving $J_{sc}$ and efficiency. However, when the thickness of the absorber exceeds the carriers transport distance, the recombination of carrier increases significantly, leading to a deterioration in cell performance. Furthermore, the material cost rises with the thickness increase. Therefore, the optimal thickness for the absorber should be 1.5 μm. The optimal device possesses $V_{oc}$ of 0.85 V, $J_{sc}$ of 30.91 mA/cm$^2$, FF of 68.05 %, and efficiency of 17.91 %. To further realizes CZTSSe solar cells with high efficiency, the series resistance should be kept below 2 Ω·cm$^2$, and the shunt resistance should be maintained above 600 Ω·cm$^2$.

## CRediT authorship contribution statement

**Yaowei Wei:** Conceptualization, Investigation, Writing - original draft, Writing - review & editing, Supervision. **Zhao Ma:** Data curation, Validation, Writing – review & editing. **Xiaoyang Zhao:** Investigation, Methodology, Writing – original draft. **Jianghao Yin:** Validation, Visualization. **Yingying Wu:** Conceptualization, Validation. **Leng Zhang:** Conceptualization, Writing – review & editing, Supervision.

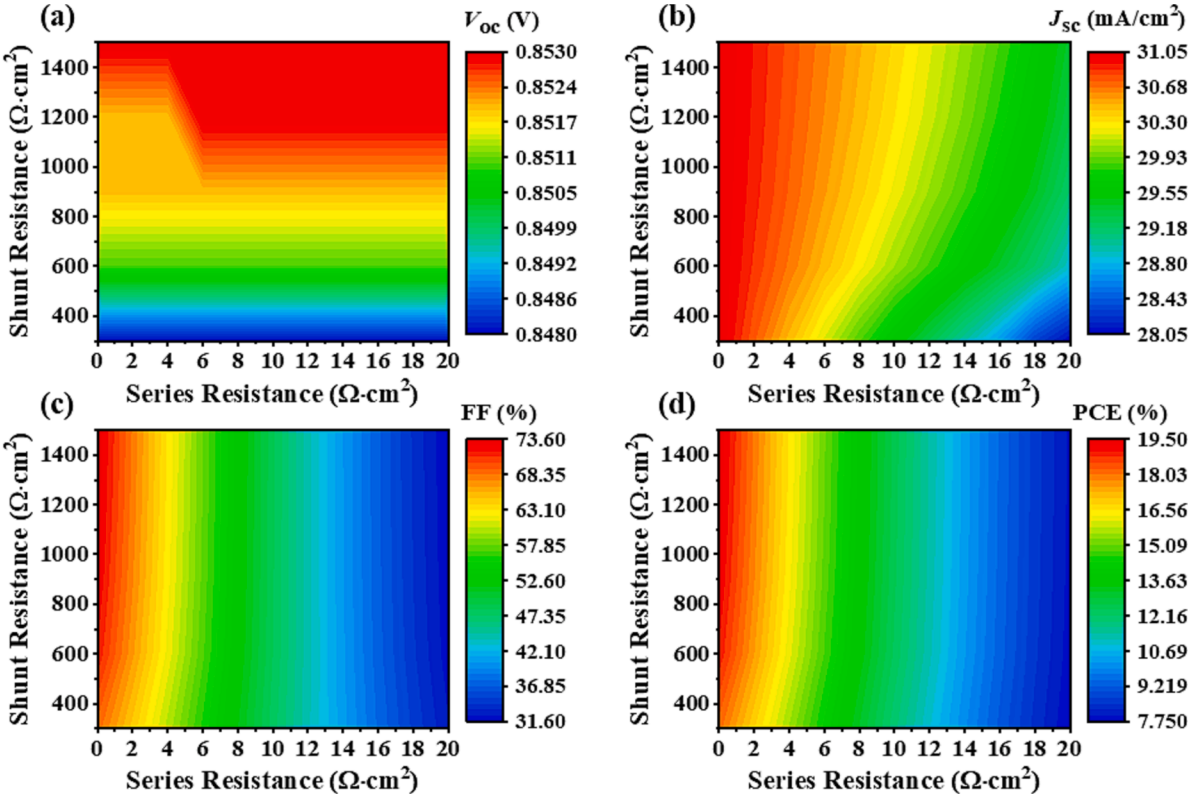


**Fig. 9.** Effects of series and shunt resistance on performance of solar cells: (a) $V_{oc}$, (b) $J_{sc}$, (c) FF, and (d) PCE.

**Ming Zhao:** Formal analysis, Writing – review & editing, Supervision.

## Declaration of competing interest

The authors declare that they have no known competing financial interests or personal relationships that could have appeared to influence the work reported in this paper.

## Data availability

Data will be made available on request.

## Acknowledgements

The authors are grateful for the support of the National Natural Science Foundation of China (Grant No. 62004175) and the Key Scientific Research Project of Colleges and Universities in Henan Province, China (Grant No. 21A430035).

## References

[1] P. Tian, L. Tang, K.S. Teng, J. Xiang, S.P. Lau, Recent Advances in Graphene Homogeneous p-n Junction for Optoelectronics, Advanced Materials Technologies. 4 (2019) 1900007, https://doi.org/10.1002/admt.201900007.
[2] F. Encinas-Sanz, J.M. Guerra, Laser-induced hot carrier photovoltaic effects in semiconductor junctions, Prog. Quant. Electron. 27 (2003) 267–294, https://doi.org/10.1016/S0079-6727(03)00002-8.
[3] R. Frisenda, A.J. Molina-Mendoza, T. Mueller, A. Castellanos-Gomez, H.S.J. van der Zant, Atomically thin p-n junctions based on two-dimensional materials, Chem. Soc. Rev. 47 (2018) 3339–3358, https://doi.org/10.1039/C7CS00880E.
[4] J. Ramanujam, D.M. Bishop, T.K. Todorov, O. Gunawan, J. Rath, R. Nekovei, E. Artegiani, A. Romeo, Flexible CIGS, CdTe and a-Si: H based thin film solar cells: a review, Prog. Mater Sci. 110 (2020), https://doi.org/10.1016/j.pmatsci.2019.100619.
[5] T.D. Lee, A.U. Ebong, A review of thin film solar cell technologies and challenges, Renew. Sustain. Energy Rev. 70 (2017) 1286–1297, https://doi.org/10.1016/j.rser.2016.12.028.
[6] I. Massiot, A. Cattoni, S. Collin, Progress and prospects for ultrathin solar cells, Nat. Energy 5 (2020) 959–972, https://doi.org/10.1038/s41560-020-00714-4.
[7] Y. Lee, H.H. Tan, C. Jagadish, S.K. Karuturi, Controlled cracking for large-area thin film exfoliation: working principles, status, and prospects, ACS Appl. Electron. Mater. 3 (2021) 145–162, https://doi.org/10.1021/acsaelm.0c00892.
[8] M. Saifullah, S. Ahn, J. Gwak, S. Ahn, K. Kim, J. Cho, J.H. Park, Y.J. Eo, A. Cho, J. S. Yoo, J.H. Yun, Development of semitransparent CIGS thin-film solar cells modified with a sulfurized-AgGa layer for building applications, J. Mater. Chem. A 4 (2016) 10542–10551, https://doi.org/10.1039/C6TA01909A.
[9] J. Guo, W.H. Zhou, Y.L. Pei, Q.W. Tian, D.X. Kou, Z.J. Zhou, Y.N. Meng, S.X. Wu, High efficiency CZTSSe thin film solar cells from pure element solution: a study of additional Sn complement, Sol. Energy Mater. Sol. Cells 155 (2016) 209–215, https://doi.org/10.1016/j.solmat.2016.06.021.
[10] Y. Wei, K. Zhou, X. Meng, X. Sun, Z. Ma, Z. Li, D. Zhuang, Improving the performance of solution–based CZTSSe absorber by selenization annealing with selenium powder in argon, J. Alloy. Compd. 976 (2024), https://doi.org/10.1016/j.jallcom.2023.173123.
[11] A.D. Saragih, W. Wubet, H. Abdullah, A.K. Abay, D.H. Kuo, Characterization of Ag-doped Cu2ZnSnSe4 bulks material and their application as thin film semiconductor in solar cells, Mater. Sci. Eng. B 225 (2017) 45–53, https://doi.org/10.1016/j.mseb.2017.08.007.
[12] P.M.P. Salomé, J. Malaquias, P.A. Fernandes, M.S. Ferreira, A.F. da Cunha, J. P. Leitão, J.C. González, F.M. Matinaga, Growth and characterization of Cu2ZnSn (S, Se)4 thin films for solar cells, Sol. Energy Mater. Sol. Cells 101 (2012) 147–153, https://doi.org/10.1016/j.solmat.2012.02.031.
[13] S. Schorr, Structural aspects of adamantine like multinary chalcogenides, Thin Solid Films 515 (2007) 5985–5991, https://doi.org/10.1016/j.tsf.2006.12.100.
[14] Y. Zhang, D. Jiang, Y. Sui, Y. Wu, Z. Wang, L. Yang, F. Wang, S. Lv, B. Yao, Synthesis and investigation of environmental protection and earth-abundant kesterite Cu2MgxZn1-xSn(S, Se)4 thin films for solar cells, Ceram. Int. (2018), https://doi.org/10.1016/j.ceramint.2018.05.167.
[15] B.C. A, S. Routray, Y. Massoud, Analysis of opto-electrical, trap complexity and defect density in Cu–Zn–Ge–S/Se kesterite thin-film solar cell, Opt. Mater. 133 (2022), https://doi.org/10.1016/j.optmat.2022.112975.
[16] M. He, K. Sun, M.P. Suryawanshi, J. Li, X. Hao, Interface engineering of p-n heterojunction for kesterite photovoltaics: a progress review, J. Energy Chem. 60 (2021) 1–8, https://doi.org/10.1016/j.jechem.2020.12.019.
[17] A. Ait Abdelkadir, M. Sahal, Theoretical development of the CZTS thin-film solar cell by SCAPS-1D software based on experimental work, Mater. Sci. Eng. B 296 (2023), https://doi.org/10.1016/j.mseb.2023.116710.
[18] Sadanand, D.K. Dwivedi, F.A. Alharthi, A. El Marghany, One-step hydrothermal synthesis of Cu2ZnSn(S, Se)4 nanoparticles: structural and optical properties, Nanosci. Nanotechnol. Lett. 12 (2020) 338–344, https://doi.org/10.1166/nnl.2020.3121.
[19] W. Shockley, H.J. Queisser, Detailed balance limit of efficiency of p-n junction solar cells, J. Appl. Phys. 32 (2004) 510–519, https://doi.org/10.1063/1.1736034.
[20] J. Zhou, X. Xu, H. Wu, J. Wang, L. Lou, K. Yin, Y. Gong, J. Shi, Y. Luo, D. Li, H. Xin, Q. Meng, Control of the phase evolution of kesterite by tuning of the selenium partial pressure for solar cells with 13.8% certified efficiency, Nat. Energy 8 (2023) 526–535, https://doi.org/10.1038/s41560-023-01251-6.
[21] M.I. Ziane, H. Bennacer, M. Mostefaoui, M. Tablaoui, M. Hadjab, A. Saim, K. Bekhedda, Anisotropic optical properties of Cu2ZnSn(SxSe1−x)4 solid solutions: first-principles calculations with TB-mBJ+U, Optik 243 (2021), https://doi.org/10.1016/j.ijleo.2021.167490.
[22] S. Levcenco, D. Dumcenco, Y.P. Wang, Y.S. Huang, C.H. Ho, E. Arushanov, V. Tezlevan, K.K. Tiong, Influence of anionic substitution on the electrolyte electroreflectance study of band edge transitions in single crystal Cu2ZnSn (SxSe1−x)4 solid solutions, Opt. Mater. 34 (2012) 1362–1365, https://doi.org/10.1016/j.optmat.2012.02.028.
[23] T. Gokmen, O. Gunawan, D.B. Mitzi, Minority carrier diffusion length extraction in Cu2ZnSn(Se, S)4 solar cells, J. Appl. Phys. 114 (2013), https://doi.org/10.1063/1.4821841.
[24] S.A. Moghadam Ziabari, A. Abdolahzadeh Ziabari, S.J. Mousavi, Efficiency enhancement of thin-film solar cell by implementation of double-absorber and BSF layers: the effect of thickness and carrier concentration, J. Comput. Electron. 21 (2022) 675–683, https://doi.org/10.1007/s10825-022-01878-w.
[25] E.A. Gaulding, J.S. Mangum, S.W. Johnston, C.S. Jiang, H. Moutinho, M.J. Reed, J. A. Rand, R. Flottemesch, T.J. Silverman, M.G. Deceglie, Differences in printed contacts lead to susceptibility of silicon cells to series resistance degradation, IEEE J. Photovolt. 12 (2022) 690–695, https://doi.org/10.1109/JPHOTOV.2022.3150727.
[26] S. Gatz, T. Dullweber, R. Brendel, Evaluation of series resistance losses in screen-printed solar cells with local rear contacts, IEEE J. Photovoltaics 1 (2011) 37–42, https://doi.org/10.1109/JPHOTOV.2011.2163925.
[27] K. Pandey, A.K. Patel, R. Mishra, Numerical study on performance enhancement of CZTSSe solar cells with Cu2O and MoTe2 as hole transport layer, J. Comput. Electron. 21 (2022) 895–904, https://doi.org/10.1007/s10825-022-01900-1.
[28] A. Niemegeers, M. Burgelman, Numerical modelling of AC-characteristics of CdTe and CIS solar cells, in: Conference Record of the Twenty Fifth IEEE Photovoltaic Specialists Conference - 1996. (1996) 901–904. doi: 10.1109/PVSC.1996.564274.
[29] A. Cherouana, R. Labbani, Study of CZTS and CZTSSe solar cells for buffer layers selection, Appl. Surf. Sci. 424 (2017) 251–255, https://doi.org/10.1016/j.apsusc.2017.05.027.
[30] B.S. Sengar, V. Garg, G. Siddharth, A. Kumar, S.K. Pandey, M. Dubey, V.V. Atuchin, S. Kumar, S. Mukherjee, Improving the Cu2ZnSn(S, Se)4-based photovoltaic conversion efficiency by back-contact modification, IEEE Trans. Electron Dev. 68 (2021) 2748–2752, https://doi.org/10.1109/TED.2021.3071105.
[31] A.K. Daoudia, Y.E. Hassouani, A. Benami, Investigation of the effect of thickness, band gap and temperature on the efficiency of CIGS solar cells through SCAPS-1D, Int. J. Eng. Tech. Res. 6 (2016) 71.
[32] V. Kumar, S.K. Agawal, Physics of semiconductor devices, Phys. Today 6 (2003) 98–99, https://doi.org/10.1002/0470068329.
[33] L. Et-taya, T. Ouslimane, A. Benami, Numerical analysis of earth-abundant Cu2ZnSn(SxSe1-x)4 solar cells based on Spectroscopic Ellipsometry results by using SCAPS-1D, Sol. Energy 201 (2020) 827–835, https://doi.org/10.1016/j.solener.2020.03.070.
[34] O.K. Simya, A. Mahaboobbatcha, K. Balachander, A comparative study on the performance of Kesterite based thin film solar cells using SCAPS simulation program, Superlatt. Microst. 82 (2015) 248–261, https://doi.org/10.1016/j.spmi.2015.02.020.
[35] P.K. Kannan, M. Anandkumar, A theoretical investigation to boost the efficiency of CZTS solar cells using SCAPS-1D, Optik 288 (2023), https://doi.org/10.1016/j.ijleo.2023.171214.
[36] A. Nagaoka, K. Yoshino, Growth of CZTS Single Crystals, 2014.
[37] A. Nakane, S. Fujimoto, G.E. Jellison, C.M. Herzinger, J.N. Hilfiker, J. Li, R.W. Collins, T. Koida, S. Kim, H. Tampo, H. Fujiwara, Inorganic Semiconductors and Passivation Layers, Springer International Publishing, Cham, 2018.
[38] Y. Sun, P. Qiu, W. Yu, J. Li, H. Guo, L. Wu, H. Luo, R. Meng, Y. Zhang, S. Liu, N-type surface design for p-Type CZTSSe thin film to attain high efficiency, Adv. Mater. 33 (2021) 2104330, https://doi.org/10.1002/adma.202104330.
[39] H. Wei, Y. Li, C. Cui, X. Wang, Z. Shao, S. Pang, G. Cui, Defect suppression for high-efficiency kesterite CZTSSe solar cells: advances and prospects, Chem. Eng. J. 462 (2023), https://doi.org/10.1016/j.cej.2023.142121.
[40] O.K. Simya, A. Mahaboobbatcha, K. Balachander, Compositional grading of CZTSSe alloy using exponential and uniform grading laws in SCAPS-ID simulation, Superlatt. Microst. 92 (2016) 285–293, https://doi.org/10.1016/j.spmi.2016.02.019.
[41] K.J. Yang, D.H. Son, S.J. Sung, J.H. Sim, Y.I. Kim, S.N. Park, D.H. Jeon, J. Kim, D. K. Hwang, C.W. Jeon, D. Nam, H. Cheong, J.K. Kang, D.H. Kim, A band-gap-graded CZTSSe solar cell with 12.3% efficiency, J. Mater. Chem. A 4 (2016) 10151–10158, https://doi.org/10.1039/C6TA01558A.
[42] S. Chen, A. Walsh, J.H. Yang, X.G. Gong, L. Sun, P.X. Yang, J.H. Chu, S.H. Wei, Compositional dependence of structural and electronic properties of Cu2ZnSn(S, Se)4 alloys for thin film solar cells, Phys. Rev. B 83 (2011), https://doi.org/10.1103/PhysRevB.83.125201.
[43] S. Ji, T. Shi, X. Qiu, J. Zhang, G. Xu, C. Chen, Z. Jiang, C. Ye, A route to phase controllable Cu2ZnSn(S1−xSex)4 nanocrystals with tunable energy bands, Sci. Rep. 3 (2013) 2733, https://doi.org/10.1038/srep02733.

[44] J. He, L. Sun, S. Chen, Y. Chen, P. Yang, J. Chu, Composition dependence of structure and optical properties of Cu2ZnSn(S, Se)4 solid solutions: an experimental study, J. Alloy. Compd. 511 (2012) 129–132, https://doi.org/10.1016/j.jallcom.2011.08.099.
[45] S. Mohammadnejad, A. Baghban Parashkouh, CZTSSe solar cell efficiency improvement using a new band-gap grading model in absorber layer, Appl. Phys. A 123 (2017) 758, https://doi.org/10.1007/s00339-017-1371-x.
[46] M.E. Erkan, V. Chawla, M.A. Scarpulla, Reduced defect density at the CZTSSe/CdS interface by atomic layer deposition of Al2O3, J. Appl. Phys. 119 (2016), https://doi.org/10.1063/1.4948947.
[47] S. Enayati Maklavani, S. Mohammadnejad, Enhancing the open-circuit voltage and efficiency of CZTS thin-film solar cells via band-offset engineering, Opt. Quant. Electron. 52 (2020) 72, https://doi.org/10.1007/s11082-019-2180-6.
[48] J. Wang, J. Zhou, X. Xu, F. Meng, C. Xiang, L. Lou, K. Yin, B. Duan, H. Wu, J. Shi, Y. Luo, D. Li, H. Xin, Q. Meng, Ge bidirectional diffusion to simultaneously engineer back interface and bulk defects in the absorber for efficient CZTSSe solar cells, Adv. Mater. 34 (2022) 2202858, https://doi.org/10.1002/adma.202202858.
[49] Y. Gong, Y. Zhang, Q. Zhu, Y. Zhou, R. Qiu, C. Niu, W. Yan, W. Huang, H. Xin, Identifying the origin of the Voc deficit of kesterite solar cells from the two grain growth mechanisms induced by Sn2+ and Sn4+ precursors in DMSO solution, Energ. Environ. Sci. 14 (2021) 2369–2380, https://doi.org/10.1039/D0EE03702H.
[50] U. Farooq, U. Ali Shah, M. Ishaq, J.G. Hu, S. Ahmed, S. Chen, Z.H. Zheng, Z.H. Su, P. Fan, G.X. Liang, Defects passivation by solution-processed titanium doping strategy towards high efficiency kesterite solar cells, Chem. Eng. J. 451 (2023), https://doi.org/10.1016/j.cej.2022.139109.
[51] T. Ikegami, T. Maezono, F. Nakanishi, Y. Yamagata, K. Ebihara, Estimation of equivalent circuit parameters of PV module and its application to optimal operation of PV system, Sol. Energy Mater. Sol. Cells 67 (2001) 389–395, https://doi.org/10.1016/S0927-0248(00)00307-X.